Surface Science 243 (1991) 273–294
North-Holland

Monte Carlo simulation of the adsorption of CO on Pt(111): thermodynamic considerations for the surface configuration of adsorbed species

Kristen A. Fichthorn [1], Erdogan Gulari and Robert M. Ziff
Department of Chemical Engineering, H.H. Dow Building, University of Michigan, Ann Arbor, MI 48109, USA

Received 18 June 1990; accepted for publication 19 September 1990

We have developed a "two-site" lattice gas model which provides a theoretical framework for understanding adsorption equilibrium in systems for which the potential energy surface is inherently heterogeneous in terms of both adsorbate–adsorbate and adsorbate–potential energy surface interactions and also entropic factors associated with the existence of two types of sites. Utilizing this general framework, we have examined two model systems with general features of the CO–Pt(111) adsorption system. In the first of these models, we represent the CO–CO interaction with a repulsive dipole–dipole – dipole–image potential and in the second, with a Lennard-Jones 6–12 potential. We delineate criteria for determining the ordered ground states of each of the systems in terms of the relative magnitudes of adsorbate–adsorbate and adsorbate–potential energy surface interactions and, utilizing Monte Carlo simulations, we calculate approximate phase diagrams for each. In addition to observing the expected order–disorder phase transitions, we observe a "bridge-to-top" transition associated with the transfer of molecules from bridge to energetically favored top sites as the temperature of the system is decreased. Both models produce phase diagrams which may be inferred from LEED studies of the CO–Pt(111) system at low coverages. In addition, the dipole–dipole – dipole–image potential reproduces quantitatively the experimentally observed coverage dependence of both the heat of adsorption and the infrared frequency of linear CO, while the Lennard-Jones model fails to reproduce these trends. We have utilized our model to address several issues related to the equilibrium of the CO–Pt(111) system and we suggest avenues for future experimental study.

1. Introduction

The adsorption of CO on Pt(111) is one of the most heavily studied systems in surface science. Numerous studies of this system conducted with a variety of experimental techniques have made available a large body of information regarding the CO–Pt(111) and CO–CO interaction. The general energetics of the CO–Pt(111) interaction, characterized by the potential energy surface (PES), has been the subject of many studies [1–10] which find that the hexagonal-close-packed Pt(111) surface contains two preferred locations for CO adsorption: on top sites directly above platinum atoms and on bridge sites between two platinum atoms. CO is more strongly bound to the top sites than to the bridge locations and the two binding states are vibrationally distinct, as well. The CO–CO interaction is evident in several experimental measures characterizing the adsorption including the LEED patterns [10–14], the infrared spectrum [15–19], and the thermal desorption spectrum [3,6,10,13,20]. Together, CO–Pt(111) and CO–CO interactions govern the adsorption equilibrium of the system as a function of temperature and coverage and an understanding of this interplay, although lacking at present, is clearly a necessary component in a detailed picture of this system.

In this paper, we review our steps in the development of a "two-site" lattice gas model which

[1] Current address: Department of Chemical Engineering, 133 Fenske Laboratory, The Pennsylvania State University, University Park, PA 16802, USA.

provides a framework for understanding the complex ramifications of adsorbate–adsorbate and adsorbate–PES interactions in the CO–Pt(111) and similar systems. Utilizing this general framework, we have conducted Monte Carlo studies of two model systems representing two conflicting points of view regarding the effective interactions among chemisorbed CO molecules in the CO–Pt(111) system. In the first of these models, we represent the CO–CO interaction with a repulsive dipole–dipole – dipole–image potential and in the second, with a Lennard-Jones 6–12 potential characterizing interactions which are repulsive over very short length scales, and attractive over most length scales. We shall show that the repulsive dipole–dipole – dipole–image potential reproduces semi-quantitatively the ordering of chemisorbed species, and coverage dependence of the heat of adsorption and the infrared frequency of CO adsorbed on top sites. Although the Lennard-Jones model also depicts a phase diagram which may be inferred from LEED studies of this system, it fails to reproduce even qualitative trends seen in the coverage-dependence of the heat of adsorption and the infrared frequency of linear CO. We have utilized our model to address several unresolved issues related to the equilibrium of the CO–Pt(111) system and we suggest avenues for future study.

2. The two-site potential energy surface

A model PES for a "two-site" adsorption system can be constructed from an elementary description of the kinetics of surface diffusion. In this model, a molecule is assumed to be chemisorbed in a potential energy well whose depth is defined by the heat of adsorption and whose parabolic shape arises from the assumption that the molecule is a harmonic oscillator. With two sites available for adsorption, a potential energy curve may be constructed as depicted in fig. 1. This curve is characterized by two energies: ΔE, the energy differences between a top and a bridge site and E_B, the barrier energy to diffusion for the bridge species (the barrier for diffusion of the top species is $(E_B + \Delta E)$). In addition, two frustrated translational frequencies parallel to the surface

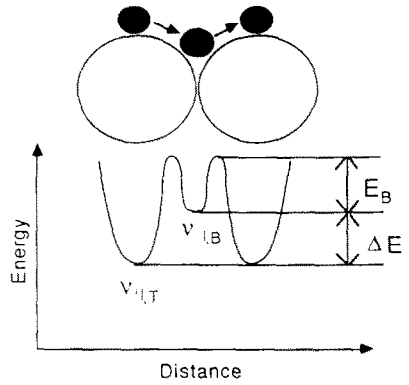

Fig. 1. The "two-site" PES is characterized by two frustrated translational frequencies parallel to the surface, $\nu_{\parallel,T}$ and $\nu_{\parallel,B}$, and two energies, ΔE, the energy difference between a top and a bridge site and E_B, the barrier energy to surface diffusion.

characterize the potential energy wells of top and bridge sites, $\nu_{\parallel,T}$ and $\nu_{\parallel,B}$, respectively. The interaction of an adsorbate with the theoretical PES shown in fig. 1 is described in terms of the Master Equation:

$$\frac{d\theta_T}{dt} = \theta_B P(T|B) - \theta_T P(B|T), \tag{1}$$

where T and B denote top and bridge sites, respectively, θ_i is the fraction of time a single species is chemisorbed on a site of type i, and $P(i|j)$ is the conditional transition probability per unit time from a site of type j to a site of type i. The transition probabilities for the Master Equation are given

$$P(T|B) = \tfrac{1}{3}\nu_{\parallel,B}\, e^{-E_B/kT}, \tag{2}$$

$$P(B|T) = \nu_{\parallel,T}\, e^{-(\Delta E + E_B)/kT}. \tag{3}$$

The factor of 1/3 in eq. (2) is included to account for the ratio of top to bridge sites on the hexagonal-close-packed Pt(111) surface.

When a molecule is at equilibrium on the two-site PES, the time derivative of the Master Equation is zero and, since $\theta_T + \theta_B = 1$, the detailed balance condition arises:

$$\frac{(1-\theta_T)}{3\theta_T} = \frac{\nu_{\parallel,T}}{\nu_{\parallel,B}} e^{-\Delta E/kT}. \tag{4}$$

Rearranging, we obtain a description of adsorption on the model PES in terms of the relative occupation of top sites

$$\theta_T(T) = \frac{1}{1 + 3\alpha\, e^{-\Delta E/kT}}, \tag{5}$$

with

$$\alpha = \frac{\nu_{\parallel,T}}{\nu_{\parallel,B}}. \tag{6}$$

Eq. (5) describes the equilibrium of molecules on a general, two-site PES at low coverages for which adsorbate–adsorbate interactions are negligible.

Different constant values of the frustrated translational frequencies of the top and bridge sites reflect the different densities of the energy levels of these chemically distinct species. For the CO–Pt(111) system, it has been observed experimentally [8] that $\nu_{\parallel,T} < \nu_{\parallel,B}$ and, thus, $\alpha < 1$. Therefore, the energy levels of the top species are lower than those of the bridge (because the top site is favored energetically) and they are also more dense. It can be seen from eq. (5) that as the temperature of the system approaches zero, the energetic contribution to the equilibrium of the system increases and, at $T = 0$, the system reaches an equilibrium which energetic considerations would dictate (i.e. all molecules on top sites). On the other hand, as $T \to \infty$, the top species is, again, slightly favored over the bridge by its density of states. However, there are three times as many bridge sites as top sites on the Pt(111) surface. Thus, the factor 3α reflects the entropy of adsorption. We shall show presently that this factor plays an interesting and nontrivial role in determining several properties of the equilibrium CO–Pt(111) system.

Studies which have focused on characterization of the CO–Pt(111) PES [6,7,10,20] have estimated values for the difference between the heat of adsorption of a top and bridge site (ΔE on fig. 1) between 8 [20] and 0.5 kcal/mol [10], although estimates are heavily skewed towards the lower value. In our studies, we examined two potential energy curves, one with $\Delta E = 0.5$ kcal/mol and one with $\Delta E = 1.0$ kcal/mol. Corresponding values of α were $\alpha = 0.1$, a choice based on the thermal helium scattering data and normal mode analysis of Lahee et al. [8], and $\alpha = 1.0$ for comparison.

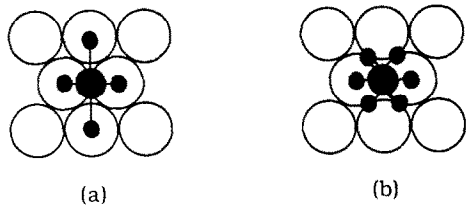

Fig. 2. (a) Lahee et al. [8] have suggested that the bridge species has two frustrated translational modes, directed as shown in the diagram. (b) The assumed isotropic frustrated translations in our model.

Some further comments are in order regarding the relationship of our model PES to the CO–Pt(111) adsorption system. One of these is that the frustrated translational frequencies are isotopic in the three directions allowed by the hexagonal-close-packed Pt(111) symmetry. While this assumption may be valid for a CO molecule diffusing from a top site, it is perhaps unsatisfactory for diffusion from a bridge site. Through inelastic helium atom scattering and normal mode analysis, Lahee et al. [8] have shown that it is likely that the bridge species has two orthogonal frustrated translational modes which are between the two top sites spanned by the bridge and between two top sites separated from the bridge by three-fold sites, as depicted in fig. 2. Although the exact hopping scheme is unimportant when equilibrium properties of a system are sought, anisotropy of the PES alters the equilibrium of the system by introducing a barrier as well as an additional frustrated translational frequency to the detailed balance equation. At this stage of understanding, we have opted for a less complex description and we note that our approximation contains sufficient detail to convey several macroscopic trends of the system.

3. Adsorbate–adsorbate interactions

In additions to interaction with the PES, molecules are subject to interactions with one another. Evidence for these interactions is seen in several experimental measures characterizing the CO–

Pt(111) system including the LEED patterns, the infrared spectra of linear CO, and the coverage-dependence of the heat of adsorption. However, since these results have not been uniquely interpreted as being due to either attractive of repulsive interactions, we have examined adsorption equilibria arising from each of these types of interaction.

Many of the experimentally-observed features of the CO–Pt(111) adsorption system may be attributed to repulsive adsorbate–adsorbate interactions. Perhaps the most compelling experimental evidence for this type of interaction is the coverage-dependence of the heat of adsorption. The heat of adsorption has been shown to exhibit large overall decreases with increasing coverage [3,6,10, 20,21] and appreciable decreases even at coverages less than 1/3 [22–24]. If these low-coverage decreases in the heat of adsorption can be attributed to adsorbate–adsorbate interactions (and not to the initial filling of defect sites having high heats of adsorption), then the repulsive interactions among CO molecules must extend over long length scales on the Pt(111) surface. As the origin of this long-range repulsion, we have considered dipole–dipole interactions.

It is quite possible that the static dipole moment of CO on Pt(111) is very high. From work function studies of CO adsorbed on Pt(111) and vicinal surfaces, Poelsema et al. [14] have estimated that the static dipole moment of CO on an "ideal" Pt(111) surface with a defect concentration of $< 10^{-3}$ is ~ 0.9 D. A major finding of this study is that the work function of CO on Pt(111) is extremely sensitive to the concentration of defects on the Pt(111) surface with surfaces having the lowest defect concentrations exhibiting the lowest minima in the work function (and, thus, higher average static dipole moments). The estimate of Poelsema and coworkers is considerably higher than estimates from previous studies [6,10,16], in which defects were presumably present to a greater extent. In addition to posessing a dipole moment associated with charge transfer to the surface, it is possible that chemisorbed CO also has an intrinsic dipole moment associated with its molecular structure. Thus, it is possible that dipole–dipole repulsions are significant in the CO–Pt(111) system. As will be shown, several of the experimentally-observed attributes of this system may be consistently interpreted in terms of this type of CO–CO interaction.

We have utilized a dipole–dipole – dipole–image potential to model the repulsive interactions in one of the model systems. For two parallel-oriented dipoles (as in the case for CO molecules adsorbed on Pt(111) for coverages ≤ 0.5 [25–27]) with identical dipole moments, the intermolecular potential is given:

$$\phi_{\text{dipole-dipole}}(r) = \mu^2/r^3, \tag{7}$$

where μ is the static dipole moment and r is the distance between chemisorbed molecules. Following Sheffler [28], we have also included two terms in the potential to account for dipole–image interactions:

$$\phi_{\text{dipole-image}}(r) = \mu^2\left(\frac{1}{(r^2+4d^2)^{3/2}} - \frac{d^2}{(r^2+4d^2)^{5/2}}\right). \tag{8}$$

Here, d is the dipole–image distance. The dipole–dipole – dipole–image potential contains two parameters, μ and d. From ESDIAD measurements, Kiskinova et al. [27] have estimated that the dipole–image distance in this system is $d \sim 1.0$ Å and this is the value utilized in our calculations. It should be noted, however, that the dipole–image interaction given by eq. (8) is not particularly sensitive to the dipole–image distance. We chose the static dipole moment $\mu = 1.5$ D so as to match the decrease in the heat of adsorption measured experimentally at half coverage in this system [10].

Further comments should be made regarding the assumption implicit in the dipole–dipole – dipole–image interaction potential. First, it is possible that the static dipole moments of top and bridge CO are different. Both Ertl et al. [10] and Norton et al. [6] have suggested that the bridge site has a static dipole moment which is smaller than that of a top site. Norton et al. have further postulated that the bridge dipole is oriented in a direction opposite that of the top site, with the negative end outward from the surface. However, since there is currently no clear resolution to this

issue, we have assumed that the dipole moments of both species are the same.

Another type of interaction which our study ignores completely is coverage-dependent charge transfer between the metal and the adsorbate – the so-called "chemical effect". Evidence for chemical effects in the CO–Pt(111) system is seen in the downward shift with coverage of the singleton frequency of linear CO observed with IR spectroscopy [15,19] and also in the coverage-dependence of the work function [6,10,14,16]. Coverage-dependent charge transfer leads to a weakening of the CO–metal bond and to changes in the dipole moment of CO with coverage. In a recent publication, Ueba [29] has utilized the coherent potential approximation to model the effect of coverage-dependent charge transfer and depolarization of CO chemisorbed on a variety of metals, including Pt(111). This model was successful in elucidating qualitative trends in the coverage dependence of the singleton frequency and the work function of CO on the different metals. Through the merging of efforts such as ours and those of Ueba, which do not strictly account for equilibrium arising from adsorbate–adsorbate and adsorbate–PES interactions, we would undoubtedly gain a more accurate description of the CO–Pt(111) system.

In addition to examining the effects of the dipole–dipole – dipole–image potential on the equilibrium properties of our model system, we have also investigated the equilibrium resulting from a Lennard-Jones 6–12 potential

$$\phi(r) = 4\epsilon\left[\left(\frac{\sigma}{r}\right)^{12} - \left(\frac{\sigma}{r}\right)^{6}\right], \tag{9}$$

where ϵ and σ are adjustable parameters. Although there is no strict physical basis for this type of interaction among chemisorbed molecules, the Lennard-Jones potential can be regarded as qualitatively depicting adsorbate–adsorbate interactions which are weakly attractive over long length scales and strongly repulsive over shorter length scales. As will be discussed subsequently, our choice of parameters for this potential was based on energetic considerations for the ground states of this system near half coverage. In past studies, several experimentally measured attributes of the CO–Pt(111) system have been attributed to attractive CO–CO interactions, including the LEED patterns [3], the IR spectrum of linear CO [17,18], and the coverage dependence of the sticking coefficient [3]. However, we shall show that this potential is incapable of consistently reproducing equilibrium properties of the CO–Pt(111) system.

4. Monte Carlo simulation of the model systems

To generate equilibrium surfaces satisfying the constraints of our model systems, we have utilized a modified version of the Metropolis algorithm [30]. In this algorithm, we begin with a random initial configuration of molecules on a lattice with two types of adsorption sites representing the Pt(111) surface and we change the positions of the molecules as equilibrium considerations dictate. Simulations were run on 32×32 lattices with periodic boundary conditions. With our chosen parameters for the dipole–dipole and Lennard-Jones potentials, the finite size of the simulation lattices did not appear to pose any problems regarding the long-range nature of the adsorbate interactions – the Lennard-Jones potential diminished to zero within a few lattice spacings, while the dipole–dipole potential reduced to less than 5 cal/mol at distances of 16 platinum diameters. Movement of the species on the simulation surfaces is accomplished as follows:

(1) A vacant (v) and an occupied (o) site are selected at random.

(2) The energy of each molecule as a result of its interaction with other adsorbed species and its position on the PES is calculated. The energy of a molecule i, E_i, is defined

$$E_i = \sum_{j \neq i} \phi(i, j) - I_T(i)\, \Delta E, \tag{10}$$

where

$$I_T(i) = \begin{cases} 0, & \text{if site } i \text{ is a bridge site} \\ 1, & \text{if site } i \text{ is a top site.} \end{cases} \tag{11}$$

and $\phi(i, j) = \phi(r_{i,j})$ is the pairwise adsorbate–adsorbate interaction potential between two mole-

cules, i and j, as given by eqs. (7) and (8) or eq. (9).

(3) The probability to move the molecule from the occupied to the vacant site is calculated:

$$P(\mathrm{v}\,|\,\mathrm{o}) = \begin{cases} \alpha\, \mathrm{e}^{-(E_\mathrm{v}-E_\mathrm{o})/kT}, \\ \quad \text{if o is a top site and v is a bridge,} \\ \mathrm{e}^{-(E_\mathrm{v}-E_\mathrm{o})/kT}, \quad \text{else,} \end{cases} \tag{12}$$

If the right-hand side of eq. (12) is greater than 1, then $P(\mathrm{v}\,|\,\mathrm{o})$ is equal to unity.

(4) The decision to accept or reject the move is based on the comparison of this probability to a random number, $r \in (0 \ldots 1)$. If r is less than $P(\mathrm{v}\,|\,\mathrm{o})$, then the move is made.

The ensemble equilibrium of adsorbed species is indicated by the attainment of a constant (minimum) surface configurational energy with "time", which can be defined as the number of attempts to exchange occupied and vacant sites. The surface configurational energy is defined

$$E_\mathrm{config} = \sum_i \sum_{j \le i} \phi(i, j) + I_\mathrm{T}(i)\, \Delta E, \tag{13}$$

where $I_\mathrm{T}(i)$ is as defined in eq. (11). Thus, by monitoring the surface configurational energy as a function of time, we recognized the achievement of equilibrium.

To generate series of surfaces at varying temperatures for fixed coverages and to facilitate the attainment of equilibrium at lower temperatures, we simulated quenching of the surfaces. In the quench simulations, we began with a random configuration of molecules at 450 K, which is roughly the desorption temperature of CO, and we decreased the temperature of the system, slowly and reversible in 20 K increments, until equilibrium at the lowest temperatures was reached. We confirmed the attainment of equilibrium at each quench stage by monitoring the configurational energy of the system, as defined by eq. (13), as a function of time. Equilibration times ranged from ~ 100,000 steps at low coverages to as many as 10 million steps at half coverage. We measured several properties of the equilibrium surfaces generated with our simulations and, in the remainder of this paper, we shall discuss these results and their pertinance to the experimental data available for the CO–Pt(111) adsorption system. Our discussion will center largely on the dipole–dipole model, while results from the Lennard-Jones model will be presented for comparison.

5. Ordering of CO on Pt(111)

Perhaps the most direct evidence of the interactions among CO molecules chemisorbed on Pt(111) is seen in the LEED patterns of this system. The first solid evidence of these patterns was presented in the pioneering study of Ertl et al. [10]. They observed a diffuse $(\sqrt{3} \times \sqrt{3})\mathrm{R}30^\circ$ diffraction pattern for this system at room temperature after the surface had been exposed to 1 L. Although the pattern sharpened somewhat as the temperature was decreased, it was still diffuse at 170 K, the lowest temperature accessible in the study, indicating a substantial degree of disorder. At 2 L exposure, Ertl observed a c(4 × 2) pattern which was sharp at temperatures below 270 K and which gradually faded as the temperature was raised to 350 K, indicating an order–disorder phase transition. At exposures above 2 L, Ertl et al. observed a gradual distortion of the c(4 × 2) pattern which they associated with "compression" of the overlayer, an observation which sparked the later "compression" [2] – "fault-line" [5] controversy concerning the structure of the overlayer at coverages > 0.5.

The experimental results of Ertl et al. at half coverage have been reproduced and refined by several groups. The c(4 × 2) structure is depicted in fig. 3a. This structure has been confirmed by the LEED analyses of Ogletree et al. [11], Hopster and Ibach [12], Hayden and Bradshaw [13], and Steininger et al. [3]. In the latter two investigations, the c(4 × 2) pattern was observed at coverages below 0.5, with Steininger et al. reporting the pattern for coverages as low as 0.35. At this coverage, Steininger et al. observed the gradual emergence of the c(4 × 2) pattern at 100 K and concluded that chemisorbed CO is highly mobile at this temperature and that the net interactions among CO molecules are attractive. Since thermal helium scattering [31] and LITD [32] studies have

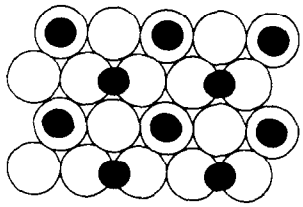

(a)

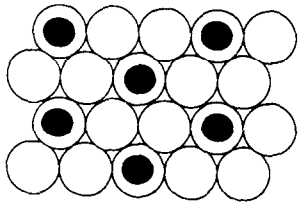

(b)

Fig. 3. The c(4×2) structure (a) and the $(\sqrt{3} \times \sqrt{3})R30°$ structure (b).

both estimated that the activation energy for the diffusion of CO on Pt(111) is ~ 7 kcal/mol with a preexponential factor of $\sim 10^{-4}$ cm^2/s, it is unlikely that CO is highly mobile at 100 K. However, the observations of Steininger et al. are perhaps consistent with other studies [10,20,21,33–35] offering evidence for the existence of an extrinsic precursor species in the CO–Pt(111) system, since such a species could be mobile at low temperatures and could potentially falsify coverage-exposure calibration. The existence of a precursor would also eliminate the need to assume that $c(4 \times 2)$ islands are formed due to attractive CO interactions, since the surface coverage in this situation would be higher that 0.35. Nevertheless, as we shall discuss subsequently, it is possible for the $c(4 \times 2)$ pattern to form at all coverages between 1/3 and 1/2 *in the absence of attractive interactions*. However, additional experimental work is necessary to clarify the range of coverages for which the $c(4 \times 2)$ pattern is present.

The low-coverage $(\sqrt{3} \times \sqrt{3})R30°$ pattern observed by Ertl et al. has also been seen by Hopster and Ibach [12] and Hayden and Bradshaw [13], both of whom saw diffuse patterns at temperatures as low as 150 K. The $(\sqrt{3} \times \sqrt{3})R30°$ pattern saturates the surface at a coverage of 1/3 and is comprised of CO molecules adsorbed on top sites, as shown in fig. 3b. Steininger et al. [3] and Poelsema et al. [14] have contested the findings of Ertl et al. with reported discrepancies in the coverage for which the work function exhibits a minimum. Ertl et al. claimed that the $(\sqrt{3} \times \sqrt{3})R30°$ pattern coincides with a minimum in the work function at a coverage of 1/3. However, Steininger et al. and Poelsema et al. have both claimed that this minimum occurs at coverages less than 1/3 and, thus, that the pattern seen by Ertl et al. was mistakenly characterized as a diffuse $(\sqrt{3} \times \sqrt{3})R30°$ pattern. Instead of this pattern, Steininger et al. have postulated the existence of another superstructure; however, they were unable to assign a real space model to this pattern. Both Steininger et al. and Poelsema et al. further claim to have observed two additional low-coverage superstructures to which they were unable to assign real-space models. To add to the controversy, Hayden and Bradshaw [13] failed to detect these patterns despite their reported efforts to reproduce the experimental results of Steininger et al. [3]. In a fairly recent study, Tüshaus et al. [15] have suggested that the low-coverage superstructures seen by Steininger et al. and Poelsema et al. may correspond to structures with local $(\sqrt{3} \times \sqrt{3})R30°$ and global (4×4) and (8×8) symmetry. As we shall show presently, a number of low coverage patterns could provide alternate explanations for the low coverage superstructures seen experimentally in the CO–Pt(111) system.

As indicated in the preceding discussion, it is not clear at which coverage $c(4 \times 2)$ domains begin to form. If adsorbate–adsorbate interactions in the CO–Pt(111) system are isotropic (as the $(\sqrt{3} \times \sqrt{3})R30°$ pattern might indicate), then the *absence* of hexagonal patterns provides information regarding the relative energies of the adsorbate–adsorbate interactions and the energy difference between top and bridge sites. When ordering in the $(\sqrt{3} \times \sqrt{3})R30°$ pattern is completed at a coverage of 1/3, the molecules must seek new minimum energy configurations as the coverage is increased. If the top and bridge sites had the same adsorption energies, then, in the presence of repulsive adsorbate interactions, minimization of energy would occur through maximization of inter-

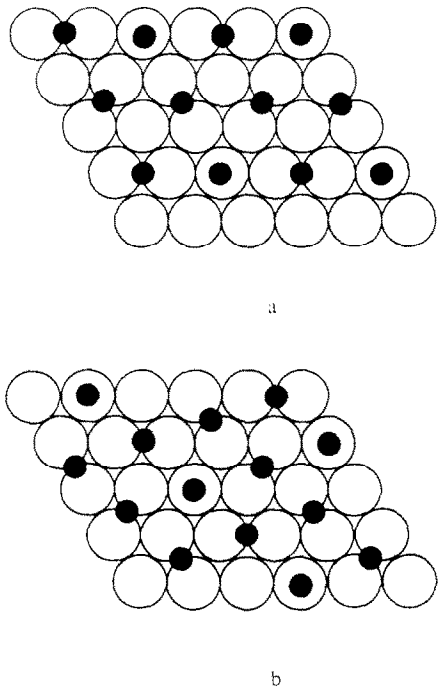

Fig. 4. The $(3/2\times3/2)$ (a) and $(\sqrt{7}/2\times\sqrt{7}/2)$R40° (b) patterns which saturate the surface at coverages of 4/9 and 4/7, respectively. These patterns may be expected to arise at coverages near 1/2 in the absence of an energetic bias for adsorption on top sites, as the ratio of top to bridge sites in both patterns is 1 : 3.

molecular distances. Two such patterns would result in this case: the $(3/2 \times 3/2)$ pattern, which saturates the surface at a fractional coverage of 4/9 and the $(\sqrt{7}/2 \times \sqrt{7}/2)$R40° pattern, which saturates the surface at a coverage of 4/7. As depicted in fig. 4, the ratio of top to bridge sites in these patterns is 1 : 3, whereas in the $c(4 \times 2)$ pattern, the ratio of top to bridge sites is 1 : 1. Therefore, the $c(4 \times 2)$ pattern will occur instead of the $(3/2 \times 3/2)$ if the more repulsive adsorbate–adsorbate interactions at the shorter $c(4 \times 2)$ distances are more than offset by the lower energy of adsorption at a top site. It should be noted, however, that if the energy difference between top and bridge sites is very large compared to the adsorbate–adsorbate interaction energy, then molecules would adsorb exclusively on top sites, as energy minimization would occur in that way.

The preceding discussion suggests a set of criteria for the relative magnitudes of interactions allowable in the model system. To investigate these criteria, we have generated surfaces with $(3/2 \times 3/2)$, $c(4 \times 2)$, $(\sqrt{7}/2 \times \sqrt{7}/2)$R40°, and (1×1) patterns and calculated the average energy of a molecule adsorbed in each of these configurations as a function of the static dipole moment, μ in eqs. (7) and (8), and ΔE, the energy difference between a top and bridge site, as depicted in fig. 1. Fig. 5 depicts the results of these calculations, indicating that, with dipole–dipole interactions, the $c(4 \times 2)$ pattern can be seen between coverages of 4/9 and 1/2 for a wide range of μ and ΔE, as depicted in regions II and III on the graph. For sufficiently large values of ΔE, depicted in region II on the graph, the $c(4 \times 2)$ pattern is favored over the $(3/2 \times 3/2)$ and, thus, it is possible to see the $c(4 \times 2)$ pattern at coverages between 1/3 and 1/2 in this parameter regime. For our chosen

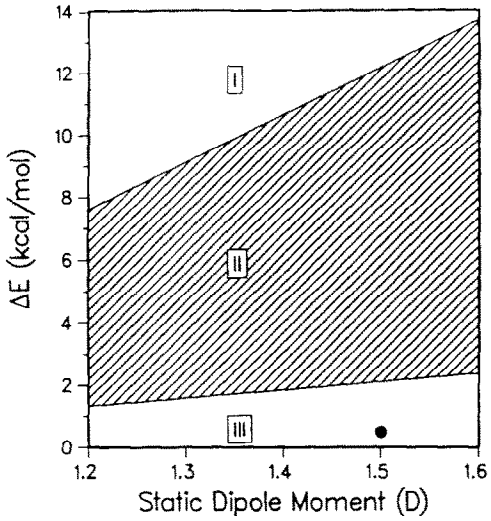

Fig. 5. A parameter diagram depicting regions in parameter space in which ordering in the $c(4\times2)$ pattern will (not) occur. (I) in this region, minimization of energy occurs through adsorption on top sites, as ΔE is large compared to the strength of the repulsive interactions. Therefore, ordering in the $c(4\times2)$ pattern will not occur. (II) ΔE is sufficiently large so that the $c(4\times2)$ pattern is favored over the $(3/2\times3/2)$ pattern shown in fig. 4. Thus, the $c(4\times2)$ pattern can be observed at coverages between 1/3 and 1/2. (III) In this region, the $c(4\times2)$ pattern is energetically favored for coverages between 4/9 and 1/2. The data point on the diagram shows the parameters utilized in this study.

values of μ and ΔE, it can be seen on fig. 5 that our model system tends to ground states with the c(4 × 2) pattern at coverages between 4/9 and 1/2.

Our simulations produced the patterns which the experimental studies have indicated (i.e. the $(\sqrt{3} \times \sqrt{3})$R30° pattern at coverages near 1/3 and the c(4 × 2) pattern near 1/2 coverage) plus several low-coverage patterns. Although fig. 5 indicates that the (3/2 × 3/2) pattern is favored energetically at coverages near 4/9, we did not observe this pattern for temperatures down to 10 K, the lowest temperature investigated. As will be discussed in more detail subsequently, we attribute our failure to observe this pattern to limitations arising from the low value of α (= 0.1) utilized in the model. Our simulations have also provided insight to pattern formation in systems with repulsive dipole–dipole interactions and have allowed us to address the following issues related to the CO–Pt(111) system:

(1) The diffuseness of the $(\sqrt{3} \times \sqrt{3})$R30° pattern at 1/3 coverage [10,12,13].

(2) The low-coverage superstructures [3,14,15].

(3) The streaks which have been reported [3,10] to emerge in the c(4 × 2) LEED pattern at coverages greater than 1/2.

Fig. 6 depicts an equilibrium simulation surface generated at $\theta = 1/3$ and $T = 110$ K. On this surface, ordering in the $(\sqrt{3} \times \sqrt{3})$R30° pattern is nearly complete. A tool which was useful in quantifying the extent of ordering on the simulation surfaces is the autocorrelation function, which is defined:

$$g(\boldsymbol{r}) = \langle n(\boldsymbol{r}^*) n(\boldsymbol{r}^* + \boldsymbol{r}) \rangle, \tag{14}$$

where

$$n(\boldsymbol{r}) = \begin{cases} 0, & \text{if site is not occupied,} \\ 1, & \text{if site is occupied,} \end{cases} \tag{15}$$

and $\langle \cdots \rangle$ denotes an average over all $\boldsymbol{r}^*$. Fig. 7 shows our measured autocorrelation function for the surface depicted in fig. 6. The strength of the correlations at a given length scale on the surface is indicated by the diameter of the circle at that length scale on the graph. Since the center point at (0, 0) represents correlations between a molecule and itself, this is the largest circle on the graph. To improve the statistics, we averaged all four quadrants on the surface and then "flipped" the pattern horizontally and vertically about the x and y axes and diagonally about the origin to create a complete plot. As can be seen in fig. 7, ordering is present to a significant extent, as indicated by the large size of the circles, with strong correlations to the sixth neighbor at the $(\sqrt{3} \times \sqrt{3})$R30° distances.

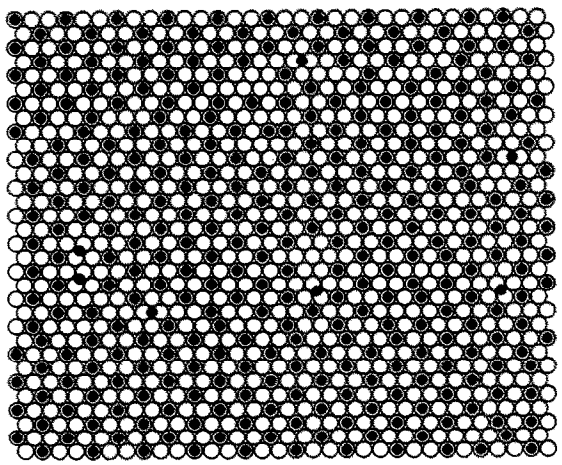

Fig. 6. An equilibrium surface generated with our algorithm at $\theta = 1/3$ and $T = 110$ K. Ordering in the $(\sqrt{3} \times \sqrt{3})$R30° pattern is nearly complete at this temperature.

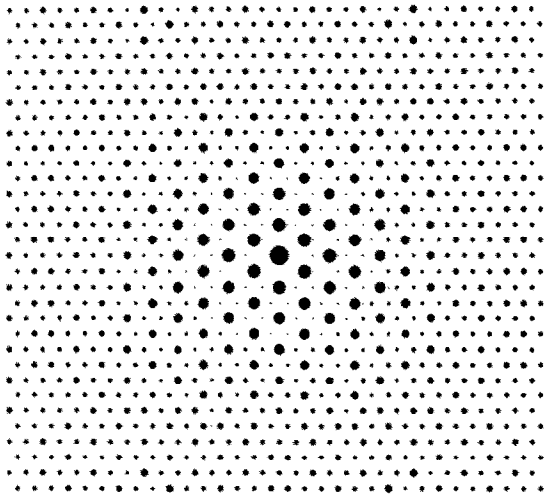

Fig. 7. The autocorrelation function for the surface of fig. 6 at $\theta = 1/3$ and $T = 110$ K. The large dots radiating from the origin (the large center dot) indicate strong $(\sqrt{3} \times \sqrt{3})$R30° correlations to the 6th neighbor.

The autocorrelation function also allows us to follow the development of correlations on the surface as a function of temperature. Fig. 8 shows the development of the $(\sqrt{3} \times \sqrt{3})R30°$ pattern as the temperature of the system is decreased from 190 K. As can be seen in this figure, we observe the commencement of the $(\sqrt{3} \times \sqrt{3})R30°$ pattern at a temperature of approximately 190 K. This structure becomes more pronounced as the temperature is decreased, however, it is still not very strong at a temperature of 150 K. These observations are qualitatively similar to those reported by Ertl et al. [10], Hayden and Bradshaw [13], and Hopster and Ibach [12]. However, unlike these experimental studies, which observe limited ordering at lower temperatures, we observe quite sharp patterns at temperatures near 130 K. One possible reason for the lack of strong $(\sqrt{3} \times \sqrt{3})R30°$ ordering in experimental systems could be diffusion limitations which prevent the attainment of equilibrium at lower temperatures. Another possible cause for the diffuseness of the $(\sqrt{3} \times \sqrt{3})R30°$ patterns observed experimentally could be that the experimental coverages were not sufficiently close to 1/3. Fig. 9 shows the autocorrelation function for a surface at a coverage of 0.30 at a temperature of 110 K. A comparison of this figure to fig. 7 reveals that the change in the extent of ordering resulting from this small change in fractional surface coverage is dramatic. We attribute this feature of our model to the repulsive interactions among the chemisorbed species which lead to pattern formation only at, or extremely close to, the exact coverage for which the pattern saturates the surface. Thus, our simulation results suggest that, with precise determination of coverages, experimental resolution of the $(\sqrt{3} \times \sqrt{3})R30°$ pattern should be greatly improved. Additional experimental work is necessary to verify this prediction.

We have also observed several low-coverage superstructures in our simulations. Fig. 10 depicts

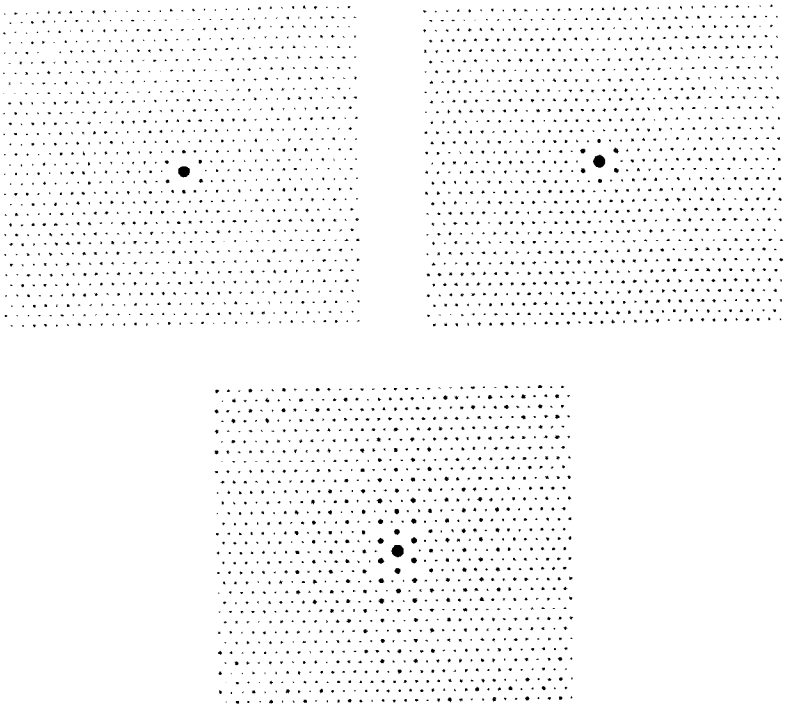

Fig. 8. The autocorrelation function of a surface at $\theta = 1/3$ and (a) $T = 190$ K, (b) $T = 170$ K, and (c) $T = 150$ K. The correlations in these figures strengthen as the temperature is decreased in a manner which is qualitatively consistent with observations reported in the literature [10,12,13].

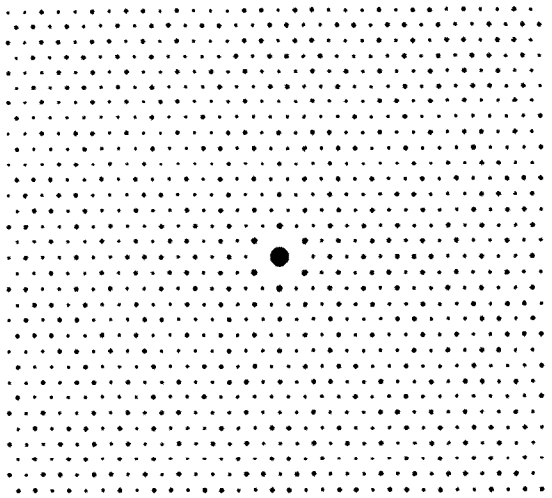

Fig. 9. The autocorrelation function of a surface at $\theta = 0.30$ and $T = 10$ K. By comparing this to fig. 6, which depicts a surface at $\theta = 1/3$ and the same temperature, we see that the reduction in ordering resulting from small changes in fractional surface coverage is dramatic. This feature of the system is characteristic of repulsive dipole–dipole interactions, which produce strong patterns only at, or extremely close to, the exact coverages for which the patterns saturate the surface.

a surface generated at $\theta = 0.2$ and $T = 10$ K and the autocorrelation function of this surface. The autocorrelation function reveals weak correlations (i.e. the six small circles near the origin) at a distance of twice the lattice spacing which are consistent with the (2×2) pattern. The (2×2) pattern saturates the surface at a coverage of $1/4$ and small domains of this pattern can be seen in fig. 10. There are also small domains of the square $(\sqrt{3} \times 2)$ pattern, which also saturates the surface at a coverage of $1/4$. However, since the hexagonal (2×2) pattern is more consistent with an isotropic potential, this is the predominant pattern in the system. Although the temperature of the surface is very low, the degree of ordering is still quite weak. As discussed above, this can be attributed to the repulsive interactions of the system. If the fractional surface coverage of the system were closer to $1/4$, the saturation coverage for this pattern, the autocorrelation function would show a strong pattern at temperatures close to and below the order–disorder transition temperature at $\theta = 1/4$ which, as will be shown subsequently is ~ 140 K.

Fig. 11 shows a surface at $\theta = 0.14$ and $T = 10$ K. The weak ordering on this surface is predominantly in the $(\sqrt{7} \times \sqrt{7})$R19.1° pattern which saturates the surface at $\theta = 1/7$. There is also some evidence for the nearly square $(\sqrt{7} \times \sqrt{7})$R40.9° pattern, which would saturate the surface at $\theta = 1/8$. Although interactions among chemisorbed species are not negligible at this coverage, changes in the potential at distances of $2\sqrt{7}$ lattice spacings are imperceptible and these ground states are highly degenerate. Given the diffusion limitations which exist in the CO–Pt(111) system, it is unlikely that either of these patterns would be observed experimentally. However, as proposed by Tüshaus et al. [15] for the (4×4) and (8×8) patterns, perhaps the low-coverage super-

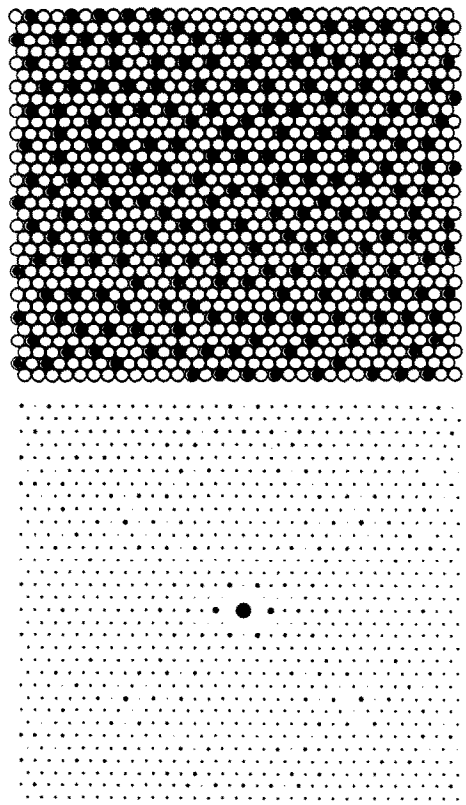

Fig. 10. A surface at $\theta = 0.2$ and $T = 10$ K and its autocorrelation function. From examination of the surface and the pattern, it can be seen that there are weak correlations at distances of two lattice spacings. The (2×2) pattern saturates the surface at $\theta = 1/4$ and stronger correlations would be expected at higher temperatures as the coverage is increased to this value.

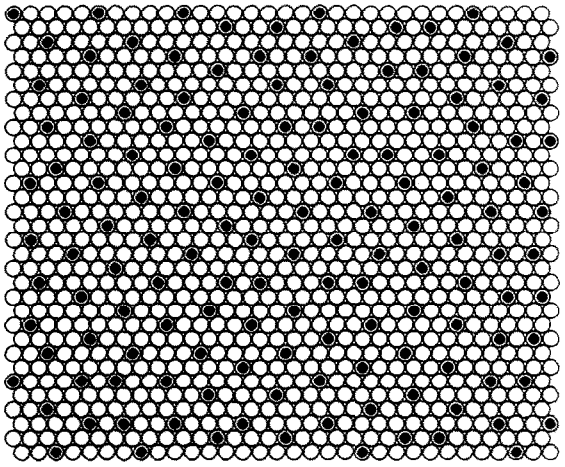

Fig. 11. A surface at $\theta = 0.14$ and $T = 10$ K. Ordering on this surface is predominantly in the $(\sqrt{7} \times \sqrt{7})$R40.9° pattern, which saturates the surface at $\theta = 1/7$. There is also evidence for the nearly-square $(\sqrt{7} \times \sqrt{7})$R19.1° pattern, which saturates the surface at $\theta = 1/8$.

structures seen in the CO–Pt(111) system with LEED can be explained in terms of the structures that we have seen with our model.

Fig. 12 depicts a surface and its autocorrelation function at half coverage and $T = 40$ K. The correlations at the c(4 × 2) distances are quite strong, indicating that the c(4 × 2) ordering is fairly extensive. Close scrutiny of the autocorrelation function reveals that many of the major spots are accompanied, to the left and right, by two minor spots, thus giving the pattern a streaked appearance. This is consistent with the formation of rows of CO molecules on top sites which will presumably evolve to "fault-line" structures [5,27] at higher coverages.

6. Order–disorder phase transitions

In the preceding section, we showed a number of surface structures produced by our model at different temperatures and coverages. In this section, we present the results of more quantitative studies of the order–disorder phase transitions of the model system. In theory, a phase transition is accompanied by singular behavior of the heat capacity with temperature. We measured the heat capacities of our surfaces as a function of temperature from the relationship:

$$C_v(T) = \frac{\langle E_{\text{config}}^2 \rangle - \langle E_{\text{config}} \rangle^2}{NkT^2}, \tag{16}$$

where E_{config} is the surface configurational energy defined in eq. (13) and N is the number of molecules in the system. Here $\langle \cdots \rangle$ denotes an average over successive configurations spaces 2000 time steps apart. Fig. 13 depicts the heat capacity versus temperature of a surface at $\theta = 0.14$. In fig. 13, two maximal, associated with two transitions of the system, can be seen. The high-temperature maximum results from an order–disorder phase transition. Although, in theory, there is a singular-

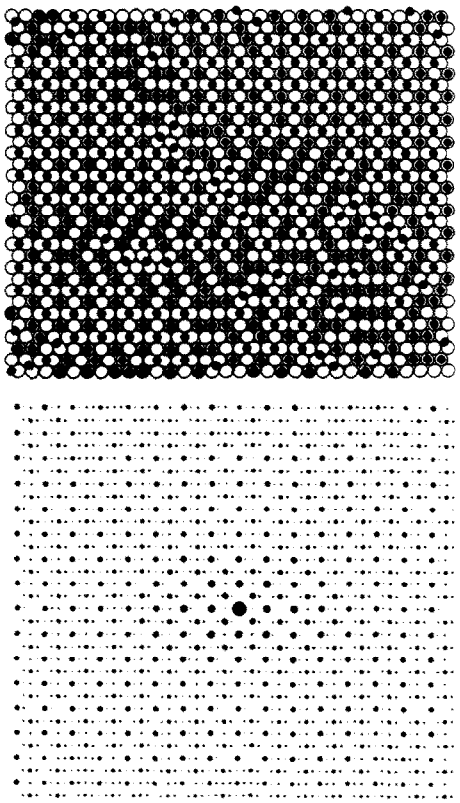

Fig. 12. A surface and its autocorrelation function at $\theta = 1/2$ and $T = 40$ K. Both the surface and the autocorrelation function show strong ordering in the c(4 × 2) pattern. The somewhat streaked appearance of the c(4 × 2) pattern is consistent with adsorption of CO molecules in rows on adjacent top sites. This structure will presumably evolve to a fault-line structure at higher coverages.

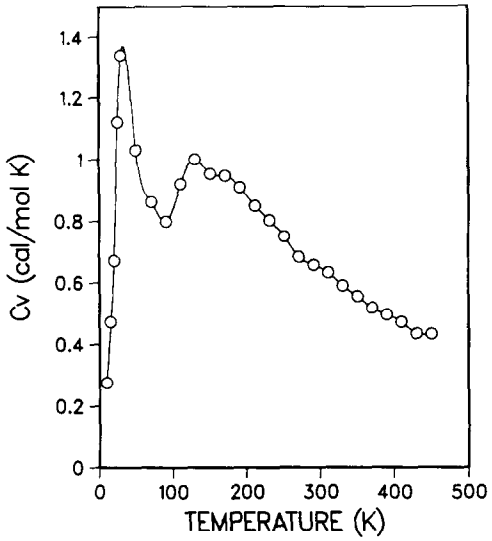

Fig. 13. The heat capacity, as calculated from eq. (16) as a function of temperature at $\theta = 0.14$. The two peaks in this curve denote two transitions of the system: a high temperature order–disorder phase transition and a low-temperature bridge-to-top transition.

ity in the heat capacity at the temperature of the transition, we observed smooth maxima in the heat capacity at the transition temperatures for all of the surfaces as a result of the finite size of the simulation lattices. The low-temperature maximum of fig. 13 arises from a bridge-to-top transition which, unlike the high-temperature maximum, does not signify a phase transition. This can be seen by examination of the behavior of a single molecule on an infinite lattice as a function of temperature. Utilizing eqs. (5) and (6) to yield the fraction of time a single molecule is adsorbed on a top site, we can calculate the energy of the molecule as:

$$E(\mathrm{T}) = (1 - \theta_{\mathrm{T}}(\mathrm{T}))\ \Delta E, \qquad (17)$$

assuming the energy of a top site is zero. Thus, the heat capacity of a molecule as a function of temperature may be calculated from eq. (16). We have calculated this quantity for $\alpha = 0.1$ and $\Delta E = 1/2$ kcal/mol and the result is depicted in fig. 14, from which it can be seen that a single molecule will undergo a bridge-to-top transition at a temperature of ~ 120 K with these parameters. However, since there is clearly no cooperativity here, this maximum does not correspond to a many-particle phase transition. We have calculated the heat capacity as a function of temperature for surfaces at a number of coverages and, from these, we have constructed an approximate phase diagram for our model system as shown in fig. 15. This figure, depicts a sharp decrease in the temperature of the bridge-to-top transition with increasing coverage and the disappearance of this transition at coverages above 0.2. We attribute this decrease to the increasing strength of adsorbate–adsorbate interactions relative to ΔE, the energy difference between a top and bridge site, as the coverage is increased. As might be expected, there is a large increase in the order–disorder transition temperature of the system as the coverage is increased. However, at intermediate coverages, the transition temperatures levels and begins to decrease as $\theta \to 1/2$. At $1/2$ coverage, calculation of the order–disorder transition temperature became unfeasible with our computing facilities and we estimated the temperature as follows: From quenching simulations, we obtained the equilibrium surface configurational energy as a function of temperature for decreasing temperatures. We also ran simulations beginning with a perfect c(4×2) surface at $1/2$

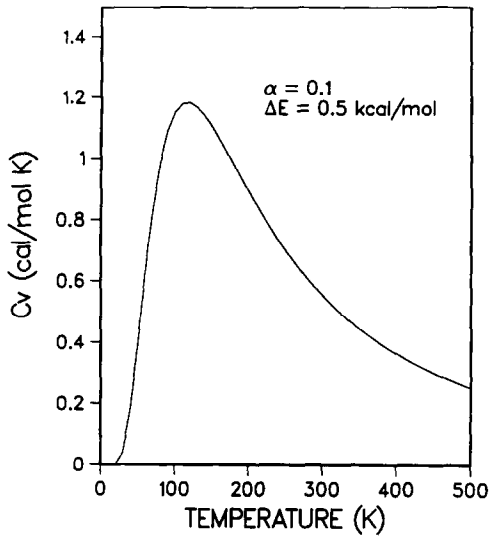

Fig. 14. The heat capacity of a single CO molecule adsorbed on an infinite Pt(111) surface as a function of temperature. The maximum in this curve denotes the bridge-to-top transition temperature.

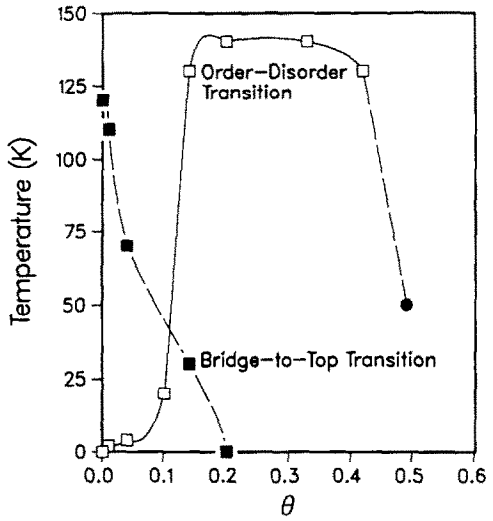

Fig. 15. A phase diagram for our model system for $\theta \leq 1/2$ which shows the temperatures and coverages of the bridge-to-top transition as well as for the order–disorder transitions. At temperatures above the order–disorder transition curve, the surface configuration of adsorbed species is generally disordered, while at temperatures below the curve, ordering is favored. The extent of ordering seen at a given coverage is also dependent on the proximity of that coverage to a coverage for which a pattern saturates the surface. The point on the diagram at half coverage is an estimate (see text).

coverage and 10 K in which we gradually heated the surface, recording the equilibrium surface configurational energy as a function of temperature. At sufficiently high temperatures, the configurational energies obtained from both sets of simulations were equal. However, at low temperatures, we observed hysteresis with the heating simulations exhibiting lower energies than the quenches. We estimated the order–disorder transition temperature of the system to be the temperature at which hysteresis first occurred – approximately 50 K.

The leveling off and decrease of the order–disorder transition temperature at intermediate to high coverages would not be expected in a system with $\alpha = 1$. Instead, we would expect to observe a decrease in the order transition temperature of the system at (theoretical) coverages closer to 1.0, where molecules are forced by limitations of the hard-sphere diameter to adsorb on top sites in the (1×1) configuration. The premature decrease in the order–disorder transition temperature observed in our model can be explained by two factors which would, either separately, or in combination, postpone the decrease in the order–disorder transition temperature to higher coverages. The first of these factors is the low value of α utilized in our simulations. With low values of α, adsorption on top sites is favored by entropy as well as by energy. This entropic bias is consistent with the energetic bias at $\theta < 1/3$, where the system tends toward ground states ($T = 0$) with all molecules adsorbed on top sites, as shown in fig. 16, which depicts the fraction of molecules adsorbed on top sites as a function of temperature for several total coverages. At $\theta > 1/3$, ground states of the system with molecules adsorbed on both bridge and top sites are favored by the energetics of adsorbate–adsorbate interactions and adsorbate–PES interactions. At these coverages, entropic and energetic factors compete. While conversions from bridge to top sites are facile, transitions from top to bridge sites are limited at low values of α (cf. eq. (12)) and adjacent top sites

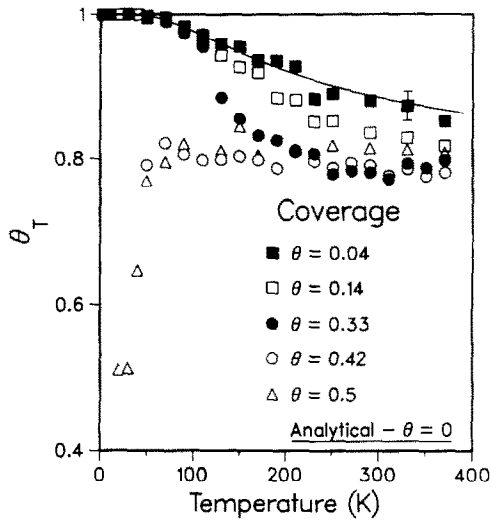

Fig. 16. The fraction of CO molecules adsorbed on top sites as a function of temperature for several total coverages. The data point with the error bar has the largest error of all the points. The analytical curve was calculated from eq. (5) with $\alpha = 0.1$ and $\Delta E = 1/2$ kcal/mol. In this figure, it can be seen that, for $\theta \leq 1/3$, the system tends to ground states with all molecules on top sites, while for higher coverages, ground states with both to and bridge sites become favored.

(in the (1 × 1) pattern) begin to be filled instead of bridge sites (in the c(4 × 2) pattern) because the entropic bias outweights the energetic factors promoting the c(4 × 2) pattern. As the temperature is decreased, transitions of molecules from bridge to higher energy nearest-neighbor top sites become less and less favored and, eventually, the order–disorder transition occurs – at a lower temperature than zero-point energetic considerations would dictate. Recently Schweizer et al. [7] have suggested that α may be higher by a factor of two than the value we have utilized. Further, α is, in actuality, an increasing function of temperature. Certainly, both of these factors would improve our high coverage description of the system, although the extent of the improvement needs to be verified.

A second factor which would induce order–disorder transitions at higher temperatures is the existence of additional short-range repulsive interactions at the nearest-neighbor distance. The dipole–dipole interaction potential is a "soft" potential in that it is not particularly steep at short distances. (However, it should be noted that the dipole–dipole potential is sufficiently steep to prevent overlap of the CO hard sphere diameters in our model.) Additional repulsive interactions at the nearest-neighbor distance would steepen the potential and, thus, they would disfavor to a greater extent the adsorption of CO molecules on nearest-neighbor top sites. This energetic bias could partially overcome the entropic bias due to low values of α.

Experimental evidence suggests that the intermolecular potential in the CO–Pt(111) system becomes very steep and is possibly discontinuous at distances of one lattice spacing. One indication of this steepness is the tilting of CO molecules adsorbed on nearest neighbor top sites observed with ESDIAD [27] as coverage is increased above 1/2. The fact that the tilting is not observed at lower coverages would indicate that repulsion at the nearest neighbor distance is significantly stronger than at other distances. Henderson et al. [35] have attributed the observed tilting of CO molecules on the steps of Pt(112) to steric limitations which clearly will only occur at the shortest CO–CO distances possible. Another indication of significantly increased repulsion at very short distances in the CO–Pt(111) system is the evolution of two peaks in the thermal desorption spectrum of this system at higher coverages [3]. Lattice gas studies [37–39] have shown that repulsive interactions lead to multiple peak thermal desorption spectra when short-range, discontinuous adsorbate–adsorbate interactions comprise the intermolecular potential. With gradual, long-range repulsive interactions, the heat of adsorption is a smooth and continuous function of coverage. Therefore, in the sole presence of these continuous interactions, multiple peaks in thermal desorption spectra would not be anticipated.

7. Coverage-dependence of the heat of adsorption

Fig. 17 shows our calculated coverage-dependence of the heat of adsorption at a temperature of 450 K as compared to coverage-dependencies measured experimentally by Seebauer et al. [21] and Ertl et al. [10]. Since adsorption is not

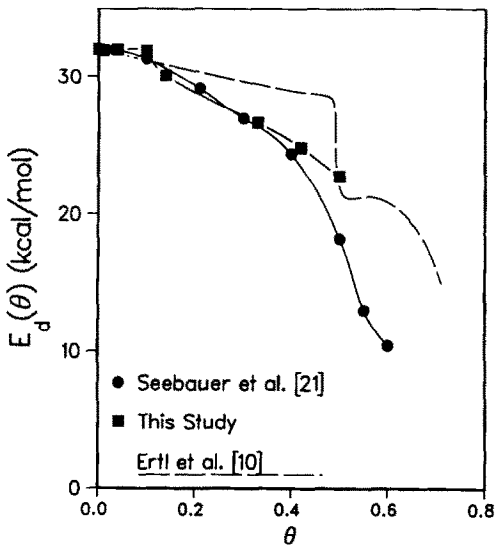

Fig. 17. The heat of adsorption as a function of coverage measured in our simulations as compared to the heats of adsorption measured experimentally in two literature studies. The line in the calculated results is to guide the eye. The fit of our calculated coverage-dependence of this parameter to the data of Seebauer et al. [21] is quite remarkable at low coverages and the overall fit of our model to the data is quite good.

activated in the CO–Pt(111) system [4,21,34,35,40], the heat of adsorption is equivalent to the activation energy for desorption. At a given coverage, we calculated the heat of adsorption as an average compiled over 2 million MCS on equilibrium surfaces. We also periodically calculated energy distributions of species in typical equilibrium configurations and these were Gaussian at all coverages. Since our Monte Carlo simulations were concerned only with energy differences on the surface, it was not necessary for us to incorporate the magnitude of the heat of adsorption in the energy calculations. In order to compare our results to those in the literature, we assumed an initial heat of adsorption of 32 kcal/mol, as measured by Ertl et al. [10] and Seebauer et al. [21]. As seen in fig. 17, agreement with the data of Seebauer et al. is remarkable up to intermediate coverages and the overall fit of the model to the experimental data is quite good. This result indicates that the low-coverage dependence of the heat of adsorption can be interpreted in terms of long-range, repulsive dipole–dipole interactions.

Another possible cause of the low-coverage decreases in the heat of adsorption measured experimentally is the initial adsorption of CO on defect sites with high heats of adsorption and subsequent filling of the Pt(111) sites, which have lower heats of adsorption. Since defects are present, to varying degrees, on all experimental single-crystal surfaces, it is desirable to assess the "error" in the predictions of our model resulting from our neglect of these sites and to explore the possibility that the experimentally-observed decreases in the heat of adsorption could be solely due to this effect. In the absence of adsorbate–adsorbate interactions and the presence of defects, the coverage-dependence of the heat of desorption should be of the form

$$E_d(\theta) = \frac{\langle E_{d,D}\rangle \theta_D}{\theta} + \frac{E_{d,0}(\theta - \theta_D)}{\theta}, \qquad (18)$$

where $E_{d,0}$ is the initial heat of adsorption on a Pt(111) site, $\langle E_{d,0}\rangle$ is the average heat of adsorption on a defect site, θ_D is the fraction of sites which are defects, and θ is the total surface coverage of adsorbed species. This expression assumes that defect sites are initially populated (i.e. $E_{d,D} > E_{d,0}$) and that $\theta \geq \theta_D$. Upon rearrangement, this expression becomes

$$E_d(\theta) = E_{d,0} + K/\theta, \qquad (19)$$

where $K = \theta_D(\langle E_{d,D}\rangle - E_{d,0})$. Thus, in the presence of defects and the absence of long-range repulsion, we would expect the heat of adsorption to decrease as $1/\theta$ with increasing θ for low coverages, where this effect would be significant. Poelsema et al. [22] have measured a linear decrease in the heat of adsorption for $\theta \leq 0.13$:

$$E_d(\theta) = E_{d,0} - \epsilon\theta. \qquad (20)$$

with $\epsilon = 16.3$ kcal/mol. In the study of Poelsema et al., the concentration of defects was estimated to be $\leq 10^{-3}$, a value which would certainly lead to a small value of K in eq. (19) for any reasonable value of $(\langle E_{d,D}\rangle - E_{d,0})$ and, thus, to a small decrease in the heat of adsorption due to defects. Low-coverage linear decreases in the heat of adsorption have also been observed in the studies of Campbell et al. [23] and Kelemen et al. [24], who both found $\epsilon = 17.0$ kcal/mol. Evidently, linear decreases in the heat of adsorption at low coverages are also found in the studies of Ertl and Seebauer, the latter of whose data is consistent with our measured slope of $\epsilon = 13.7$ kcal/mol for coverages less than 0.14.

8. IR shift of linear CO

Another experimentally measured property of the CO–Pt(111) system which we measured for our system is the IR shift which would result from dipole–dipole coupling of the linear species. We have calculated dipole-coupling shifts for equilibrium surfaces at various coverages at a temperature of 300 K so that comparisons to experimentally-measured shifts at that temperature could be made. We calculated the shifts utilizing the formalism of Sheffler [28]. Assuming a singleton frequency for linear CO of 2084 cm^{-1}, as measured by Tüshaus et al. [15] and Olsen and Masel [19], we calculated the frequency associated with

the C–O stretch normal to the surface, ν_0, with the formula

$$\nu_0 = \nu_s\left(1 - \frac{\alpha_v}{4d^3 - \alpha_e}\right)^{-1/2}. \quad (21)$$

From this, the shift in frequency with coverage is given as

$$\nu(\theta) = \nu_0\left(1 + \frac{\alpha_v\left(s(\theta) - \frac{1}{4}d^3\right)}{1 + \alpha_e\left(s(\theta) - \frac{1}{4}d^3\right)}\right)^{1/2}. \quad (22)$$

In these expressions, α_v and α_e are the vibrational and electronic polarizabilities of CO, $S(\theta)$ is the lattice sum in our potential given as the sum of Eqs. (7) and (8) divided by μ^2. There has been some discrepancy in the literature over the correct values of α_v and α_e. Mahan and Lucas [41] have utilized average values for gas phase CO, $\alpha_v = 0.057$ and $\alpha_e = 1.89$ Å^3, whereas Sheffler [28] has utilized gas phase values along the C–O axis of $\alpha_v = 0.057$ and $\alpha_e = 2.543$ Å^3. We performed calculations with both sets of parameters and found excellent agreement of our model to the experimental results of Tüshaus et al. and Olsen and Masel with the values suggested by Mahan and Lucas. Fig. 18 depicts our calculated dipole–dipole coupling shifts as compared to experimental results. The points on this curve were measured as an average over five equilibrium surfaces separated in time by 5000 steps. Our model agrees well with the experimental data at low to intermediate coverages and shows slight deviations at higher coverages, where our calculated shifts are somewhat higher than those measured experimentally. The deviations of our model at higher coverages are most likely a result of either the low value of α utilized in our simulations or the absence of strong repulsions at the nearest neighbor distance. As discussed previously, both of these factors would disfavor CO adsorption on top sites at nearest neighbor distances and would, thus, reduce the value of the lattice sum, $S(\theta)$ in eqn. (22). We have also calculated the expected shift for a perfect c(4 × 2) surface at 1/2 coverage. As seen in fig. 18, the shift arising from this structure is ~ 14 cm^{-1} less than that of our equilibrium surface at 1/2 coverage and 300 K. Although the location of this point is consistent with the trend

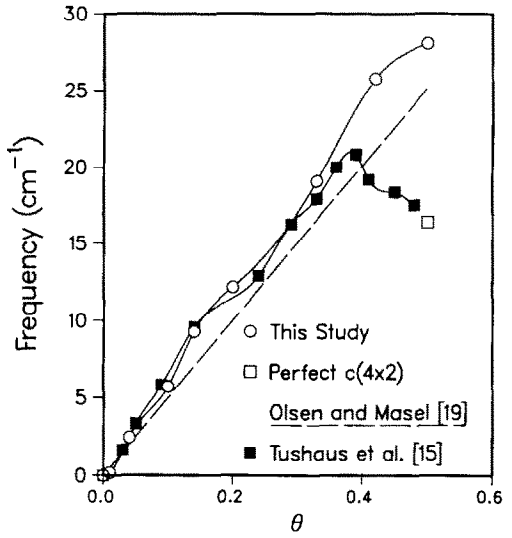

Fig. 18. The calculated IR shift of linear CO due to dipole–dipole vibrational coupling as compared to the experimental results of Tüshaus et al. [15] and Olsen and Masel [19]. The line in the calculated results is to guide the eye. Agreement of our predicted shift with the experimentally-measured shifts is quite good at low coverages, although our calculated shifts are somewhat higher than the measured shifts at intermediate coverages. The additional data point at $\theta = 1/2$ is the calculated IR shift of a perfect c(4 × 2) surface at half coverage.

observed by Tüshaus et al., it is more likely that the actual point for the CO–Pt(111) system at this coverage is somewhat higher than the perfect c(4 × 2) point. The order–disorder transition temperature of the CO–Pt(111) system at half coverage is ~ 270 K [10], indicating that the surface should be somewhat disordered at 300 K.

9. The Lennard-Jones model

We have also examined an equilibrium which would arise in our model system from Lennard-Jones 6–12 interactions of the form given in Eq. (9). The model potential energy surface for these calculations was characterized by $\Delta E = 1.0$ kcal/mol and $\alpha = 1.0$. As can be seen in eq. (9), the Lennard-Jones potential has two parameters, σ and ϵ. Through manipulation of σ, the length scales over which the potential is attractive and repulsive may be adjusted. Thus, with this potential, it is possible to observe the formation of

adsorbate islands at low coverages with densities and patterns such as the c(4 × 2) and the (1 × 1), which saturate the surface only at higher coverages. Because the repulsive range of the Lennard-Jones potential is adjustable, there are considerations for the ground states of the system at coverages below 1/3 in addition to those for coverages above 1/3 discussed in section 5. Perhaps the most peremptory restrictions we must place on the parameters of the Lennard-Jones potential is that they be physically reasonable. With this consideration, we set a lower bound on σ of 2.77 Å since, for σ less than this, molecules will be attracted at distances which violate the CO hard-sphere diameter. Another restriction which arises from this consideration is our limit of 10 kcal/mol on the strength of the repulsion a molecule can feel at the nearest neighbor distance. With $\Delta E = 1.0$ kcal/mol, there is an upper limit of ϵ for which the c(4 × 2) pattern will be favored energetically over the $(\sqrt{3} \times \sqrt{3})$R30° pattern at $\theta \leq 1/3$. A similar consideration arises for the c(4 × 2) pattern at larger values of σ: for sufficiently strong adsorbate-adsorbate interactions, the (3/2 × 3/2) and the $(\sqrt{7}/2 \times \sqrt{7}/2)$R40° patterns will be observed between coverages of 1/3 and 1/2 instead of the c(4 × 2) pattern. A final consideration for the ground states of the system arises from the fact that, with very weak adsorbate-adsorbate interactions resulting from low ϵ, adsorption on top sites in the (1 × 1) pattern will be favored over ordering, since, with $\Delta E = 1.0$ kcal/mol, the energy of the overlayer would be minimized in this way.

Fig. 19 depicts the parameter diagram which arises from these considerations. The shaded region on this figure represents values of ϵ and σ for which the experimentally observed ordering of the CO–Pt(111) system (i.e. the $(\sqrt{3} \times \sqrt{3})$R30° pattern at $\theta \leq 1/3$ and the c(4 × 2) pattern at coverages near 1/2) is energetically favored with the Lennard-Jones potential. We have chosen the boundaries on this diagram such that the c(4 × 2) pattern is favored energetically between 1/3 and 1/2 coverage. The data point on the diagram represents our chosen values of $\sigma = 3.7$ Å and $\epsilon/k = 30.0$ K.

Since α was unity in our Lennard-Jones model

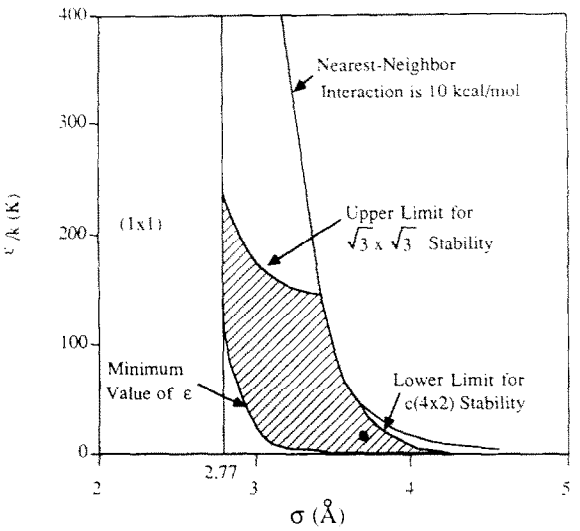

Fig. 19. The shaded region on this diagram depicts the values of ϵ and σ in the Lennard-Jones potential for which the $(\sqrt{3} \times \sqrt{3})$R30° pattern is seen for $\theta \leq 1/3$ and the c(4 × 2) pattern is seen for $1/3 < \theta \leq 1/2$ with $\Delta E = 1.0$ kcal/mol. The data point represents our chosen parameters, $\epsilon/k = 30.0$ K and $\sigma = 3.7$ Å.

system, there was no ambiguity concerning the predominant patterns at $\theta \leq 1/2$. As expected, we observed the $(\sqrt{3} \times \sqrt{3})$R30° pattern for $\theta \leq 1/3$ and coexistence of $(\sqrt{3} \times \sqrt{3})$R30° and c(4 × 2) domains up to a coverage of 1/2, where the pure c(4 × 2) pattern should be observed. Fig. 20 shows a surface and its autocorrelation function at $T = 80$ K and $\theta = 0.35$ in which there is coexistence of the $(\sqrt{3} \times \sqrt{3})$R30° and c(4 × 2) domains. The six-pointed star pattern around the origin of the autocorrelation function indicates this coexistence.

By measuring the heat capacity of our equilibrium surfaces as a function of temperature, we constructed an approximate phase diagram for the Lennard-Jones system, as depicted in fig. 21. As indicated in this figure, the Lennard-Jones model is a rich thermodynamic system. At $\theta \leq 1/3$, the system undergoes a bridge-to-top transition to a top-dominated $(\sqrt{3} \times \sqrt{3})$R30° phase whose intensity ranges from very weak at low coverages and temperatures near the bridge-to-top transition and very sharp at low temperatures and coverages near 1/3. Since the Lennard-Jones potential has an attractive portion, we observe a first-order

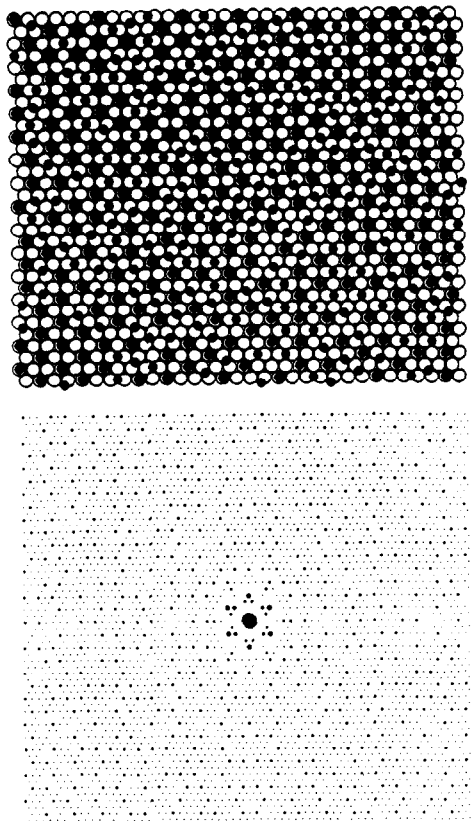

Fig. 20. A surface and its autocorrelation function at $T = 80$ K and $\theta = 0.35$. In these pictures, we see coexistence of the $(\sqrt{3} \times \sqrt{3})$R30° and c(4×2) domains. The six-pointed star pattern around the origin of the autocorrelation function indicates this coexistence.

phase transition of CO molecules into $(\sqrt{3} \times \sqrt{3})$R30° islands at very low temperatures. The appearance of the $(\sqrt{3} \times \sqrt{3})$R30° pattern in the Lennard-Jones model is consistent with the experimental observations of Ertl et al. [10], Hayden and Bradshaw [13], and Hopster and Ibach [12]. However, unlike the experimental studies of Steininger et al. [3] and Poelsema et al. [14], we did not observe any low-coverage structures with a periodicity greater than the $(\sqrt{3} \times \sqrt{3})$R30° pattern with this model. Since it can be argued that the low-coverage superstructures observed in the experimental studies arise from fragments of the $(\sqrt{3} \times \sqrt{3})$R30° pattern which cannot coalesce due to diffusion limitations at low temperatures, we could attribute our inability to see these structures to the fact that our surfaces are at equilibrium.

At $\theta > 1/3$, the bridge-to-top transition disappears since, at these length scales, adsorbate-adsorbate interactions become significantly stronger than ΔE. At these coverages, we observed a phase transition of molecules to a $(\sqrt{3} \times \sqrt{3})$R30° – c(4 × 2) coexistence phase which is pure $(\sqrt{3} \times \sqrt{3})$R30° at $\theta = 1/3$ and presumably pure c(4 × 2) at $\theta = 1/2$. Although we observed c(4 × 2) domains at half coverage, it was difficult to attain equilibrium at this coverage because of the steepness of the Lennard-Jones potential at the length scales of the c(4 × 2) pattern. However, energetic considerations indicate that, with sufficient time, the c(4 × 2) pattern will evolve at this coverage at temperatures below the order–disorder transition temperature (i.e. the configurational energy of a surface with a perfect c(4 × 2) pattern is much lower than that of our simulation surface).

Although the phase diagram predicted by the Lennard-Jones model compares favorably with the ordering seen experimentally in the CO–Pt(111) system, the other predictions of the Lennard-Jones model are in poor agreement with experimental measures. The heat of adsorption in the Lennard-Jones model is virtually constant with coverage, showing a small 2 cal/mol decrease from zero to half coverage in contrast to the rather large de-

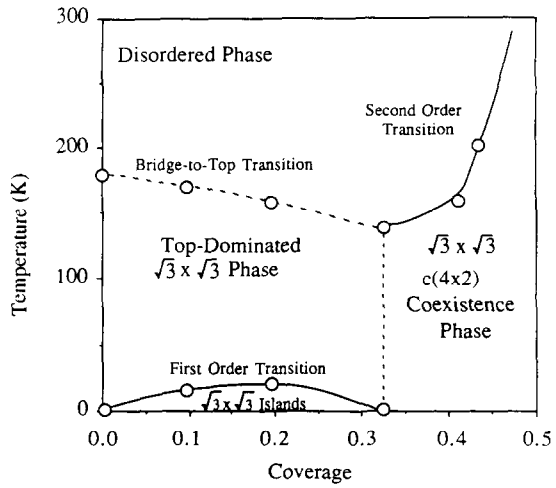

Fig. 21. The phase diagram of the Lennard-Jones model system.

crease of ~ 9 kcal/mol observed experimentally in the CO–Pt(111) system (cf. fig. 17). Since our chosen value of σ is virtually the largest value which will reproduce the experimentally-observed ordering of the CO–Pt(111) system (cf. fig. 19), indicating that the repulsive potential at half coverage is nearly as repulsive as is possible, it is highly unlikely that the Lennard-Jones potential is capable of predicting significant decreases in the heat of adsorption as a model for the CO–Pt(111) system.

Although the surface configuration of adsorbed species as a function of temperature and coverage would appear to be consistent with the experimentally-observed behavior of the CO–Pt(111) system, the IR shift predicted by this model falls below experimental determinations, as shown in fig. 22. We calculated the shifts of the Lennard-Jones potential with the procedure utilized for the surface of the dipole–dipole model. An interesting aspect of the IR shift of the Lennard-Jones model is that the calculated shift will not go to zero without a change of slope, a trend which is consistent with the early observations of King and coworkers [17,18], who attributed this phenomenon to the existence of attractive interactions among the chemisorbed molecules. Since the Lennard-Jones potential is attractive over the longer length scales, our calculated shifts confirm the prediction of these studies, although there were no well-defined islands on our simulation surfaces at temperatures of 300 K. Later studies of Tüshaus et al. [15] and Olsen and Masel [19] revealed that changes in the slope of the IR frequency of linear CO with coverage may be attributed to the initial population of defect sites with high heats of adsorption and low singleton frequencies and subsequent filling of "perfect" Pt(111) sites. Thus, the early conclusions of King and colleagues probably do not apply to the CO–Pt(111) system.

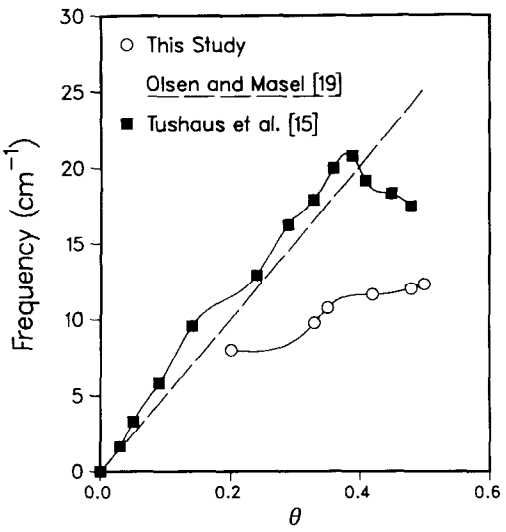

Fig. 22. The IR shift of linear CO due to dipole–dipole coupling. The line in the calculated results is to guide the eye. As can be seen, the Lennard-Jones model does not compare favorably with experiments as the shifts measured with this model are both lower in magnitude and lower in slope than the experimentally-measured shifts.

10. Conclusions

In summary, we have developed a "two-site" lattice gas model providing a theoretical framework for understanding adsorption equilibrium in systems for which the PES is inherently heterogeneous in terms of adsorbate–adsorbate and adsorbate–PES interactions and entropic factors associated with the existence of two types of sites. Utilizing this general framework, we examined two model systems with general features of the CO–Pt(111) adsorption system. In the first of these models, we represented the CO–CO interaction with a repulsive dipole–dipole – dipole–image potential and in the second, with a Lennard-Jones 6–12 potential. We delineated criteria for determining the ordered ground states of each of the systems in terms of the relative magnitudes of adsorbate–adsorbate and adsorbate–PES interactions and, utilizing Monte Carlo simulations, we calculated approximate phase diagrams for each. In addition to observing the expected order–disorder phase transitions, we observed a gradual "bridge-to-top" transition associated with the transfer of molecules from bridge to energetically favored top sites as the temperature of the system is decreased. Both models produce phase diagrams which may be inferred from LEED studies of the CO–Pt(111) system at low coverages. In addition, the dipole–dipole – dipole–image potential repro-

duced quantitatively the experimentally observed coverage dependence of both the heat of adsorption and the infrared frequency of linear CO, while the Lennard-Jones model failed to reproduce these trends.

Our efforts have reconfirmed the well-known problem of nonuniqueness of adsorbate–adsorbate interactions in reproducing experimentally observed ordering and order–disorder phase transitions of chemisorbed species. However, by matching infrared shifts and the coverage dependence of the heat of adsorption calculated from the models to experiment, we were able to support the likelihood that the CO–CO interaction in the CO–Pt(111) system is long range and substantially repulsive. The analysis presented in this paper may be applied to similar systems (e.g. CO–Ni(111), CO–Pd(111)) and shows promising potential for providing a clearer insight to adsorption in systems for which the PES is inherently heterogeneous.

Several predictions of our model are open for experimental testing. First, if adsorbate-adsorbate interactions are of a long-range repulsive nature, then pattern formation, particularly for the $(\sqrt{3} \times \sqrt{3})R30°$ pattern, occurs only at, or within approximately less than one hundredth of a monolayer of, the exact coverage for which the pattern saturates the surface. Thus, if such a precise resolution is possible, then a strong $(\sqrt{3} \times \sqrt{3})R30°$ pattern should emerge at $\theta \approx 0.33$ at temperatures below the order–disorder transition temperature. Other patterns at lower coverage could be similarly resolved if diffusion limitations can be overcome, however, the difficulty of resolving patterns will increase with decreasing coverage.

As discussed in section 3, the patterns formed between CO coverages of 1/3 and 1/2 should place a restriction on the relative magnitudes of CO–CO and CO–PES interactions and these could be investigated more thoroughly. Also, a comparison of the patterns of the CO–Pt(111), CO–Pd(111), and CO–Ni(111) systems at these coverages will reveal similarities and differences between adsorbate–adsorbate and adsorbate–PES interactions in these three systems.

Our results indicate that both energetic and entropic differences in the binding states of top and bridge CO affect the phase diagram of the CO–Pt(111) system. The relative proportions of top and bridge CO at equilibrium reflect the phase diagram and could be measured and fitted to the simple model of eq. (5) at low coverages. The high coverage ratios can be measured and compared to fig. 16. At some high-temperature limit, the ratio of top to bridge CO species should approach a constant value from which α can be obtained (cf. eq. (5)) provided that the coverage of CO is not sufficiently high as to alter the density of states of the binding sites.

Acknowledgements

Partial financial support of this project by the KCRE program of the National Science Foundation and the Horace H. Rackham Graduate School of the University of Michigan is greatfully acknowledged.

References

[1] H. Frotzheim, H. Hopster, H. Ibach, and S. Lehwald, Appl. Phys. 13 (1977) 147.
[2] A.M. Baró, and H. Ibach, J. Chem. Phys. 71 (1979) 4812.
[3] H. Steininger, S. Lehwald, and H. Ibach, Surf. Sci. 123 (1982) 264.
[4] H. Frotzheim, and M. Schulze, Surf. Sci. 211/212 (1989) 837.
[5] N.R. Avery, J. Chem. Phys. 74 (1981) 1.
[6] P.R. Norton, J.W. Goodale, and E.B. Selkirk, Surf. Sci. 83 (1979) 189.
[7] E. Schweizer, B.N.J. Persson, M. Tüshaus, D. Hoge, and A.M. Bradshaw, Surf. Sci. 213 (1989) 49.
[8] A.M. Lahee, J.P. Toennies, and Ch. Wöll, Surf. Sci. 177 (1986) 371.
[9] E. Shustorovich, Surf. Sci. Rep. 6 (1986) 1.
[10] G. Ertl, M. Neumann, and K.M. Streit, Surf. Sci. 64 (1977) 393.
[11] D.F. Ogletree, M.A. Van Hove, and G.A. Somorjai, Surf. Sci. 173 (1986) 351.
[12] H. Hopster, and H. Ibach, Surf. Sci. 77 (1978) 109.
[13] B.E. Hayden, and A.M. Bradshaw, Surf. Sci. 125 (1983) 787.
[14] B. Poelsema, R.L. Palmer, and G. Comsa, Surf. Sci. 123 (1982) 152.
[15] M. Tüshaus, E. Schweizer, P. Hollins, and A.M. Bradshaw, J. Electron. Spectrosc. Relat. Phenom. 44 (1987) 305.

[16] K. Horn, and J. Pritchard, J. Phys. (Paris) 38 (1977) C4-164.
[17] A. Crossley, and D.A. King, Surf. Sci. 68 (1977) 528.
[18] A. Crossley, and D.A. King, Surf. Sci. 95 (1980) 131.
[19] C.W. Olsen, and R.I. Masel, Surf. Sci. 201 (1988) 444.
[20] R.W. McCabe, and L.D. Schmidt, Surf. Sci. 65 (1977) 189.
[21] E.G. Seebauer, A.C.F. Kong, and L.D. Schmidt, Surf. Sci. 176 (1986) 134.
[22] B. Poelsema, R.L. Palmer, and G. Comsa, Surf. Sci. 136 (1984) 1.
[23] C.T. Campbell, G. Ertl, J. Kuipers, and J. Segner, Surf. Sci. 107 (1981) 257.
[24] S.R. Kelemen, T.E. Fisher, and J.A. Schwarz, Surf. Sci. 81 (1979) 440.
[25] D.A. Wesner, F.P. Coenen, and H.P. Bonzel, J. Vac. Sci. Technol. A 5 (1986) 927.
[26] M. Trenary, S.L. Tang, R.J. Simonson, and F.R. McFeely, Surf. Sci. 124 (1983) 555.
[27] M. Kiskinova, A. Szabó, and J.T. Yates, Jr., Surf. Sci. 205 (1988) 215.
[28] M. Sheffler, Surf. Sci. 81 (1979) 443.
[29] H. Ueba, Surf. Sci. 188 (1989) 421.
[30] N. Metropolis, A.W. Rosenbluth, A.H. Teller, and E. Teller, J. Chem. Phys. 21 (1953) 1087.
[31] B. Poelsema, L.K. Verheij, and G. Comsa, Phys. Rev. Lett. 49 (1982) 1731.
[32] E.G. Seebauer, A.C.F. Kong, and L.D. Schmidt, Diffusion and Convention in Porous Catalysts, AIChE Symposium Series 266 (1988) 1.
[33] R.A. Shigeishi, and D. King, Surf. Sci. 58 (1976) 379.
[34] C.T. Campbell, G. Ertl, H. Kuipers, and J. Segner, Surf. Sci. 107 (1981) 207.
[35] L.K. Verheij, J. Lux, A.B. Anton, B. Poelsema, and G. Comsa, Surf. Sci. 182 (1987) 390.
[36] M.A. Henderson, A. Szabó, and J.T. Yates, Jr., preprint.
[37] M.E. Bridge, and R.M. Lambert, Proc. R. Soc. A 370 (1980) 545.
[38] D.L. Adams, Surf. Sci. 42 (1974) 12.
[39] J.L. Sales, and G. Zgrablich, Phys. Rev. B 35 (1987) 9520.
[40] T.H. Lin, and G.A. Somorjai, Surf. Sci. 107 (1981) 573.
[41] G.D. Mahan, and A.A. Lucas, J. Chem. Phys. 68 (1978) 1344.